

## Green synthesis of flower-like ZnO nanoparticles mediated by paulownia tomentosa: characterization and drug delivery performance

X. Chen, Y. Wu\*

*The First Affiliated Hospital of Ningbo University, Ningbo, Zhejiang, 315000, China*

This study reports an eco-friendly synthesis of hierarchically structured zinc oxide nanoparticles using Paulownia tomentosa leaf extract as a bio-template. The synthesized nanoparticles displayed a distinctive flower-like morphology developed through a three-stage assembly process, confirmed by time-dependent morphological analysis. BET analysis revealed a mesoporous structure with type IV isotherms and H3 hysteresis loops. Spectroscopic characterization confirmed the wurtzite crystal structure with characteristic Raman modes at  $438\text{ cm}^{-1}$  (E2-high),  $380\text{ cm}^{-1}$  (A1-TO), and  $583\text{ cm}^{-1}$  (E1-LO). Surface modification with PEG-4000 enhanced the nanoparticles' performance as drug carriers, demonstrating Korsmeyer-Peppas model release kinetics ( $R^2 = 0.992$ ) with a release exponent of 0.68. The nanostructures showed 2.3-fold higher drug loading capacity compared to conventional spherical ZnO particles. Biological evaluation revealed significant antimicrobial efficacy with inhibition zones of 28 mm against *S. aureus* and 24 mm against *E. coli* at  $100\text{ }\mu\text{g/mL}$  concentration, while demonstrating selective cytotoxicity against MCF-7 breast cancer cells with minimal effect on normal breast epithelial cells.

(Received December 12, 2024; Accepted March 14, 2025)

Keywords: Mesoporous nanomaterials, Bio-templated synthesis, Controlled release, Antimicrobial activity, Targeted therapeutics

### 1. Introduction

The rapid advancement of nanotechnology has revolutionized various fields, particularly in the development of drug delivery systems. Metal oxide nanoparticles are becoming increasingly popular due to their distinct physical and chemical characteristics, as well as their wide range of potential uses [1,2]. Zinc oxide (ZnO) nanoparticles, in particular, have garnered significant attention owing to their remarkable properties including wide bandgap (3.37 eV), large exciton binding energy (60 meV), and biocompatibility [3]. Traditional methods of nanoparticle synthesis often involve hazardous chemicals and complex procedures, raising environmental concerns and limiting their biological applications [4]. This has led to increasing interest in green synthesis approaches that utilize natural resources as reducing and stabilizing agents. Plant-mediated synthesis has emerged as an eco-friendly, cost-effective, and scalable method for producing metal oxide

---

\* Corresponding author: 15825563647@163.com

<https://doi.org/10.15251/DJNB.2025.201.275>

nanoparticles with controlled morphology and enhanced biological activity. *Paulownia tomentosa*, commonly known as the princess tree, has gained attention as a promising biological template for nanoparticle synthesis [5]. The plant is rich in a variety of bioactive compounds such as phenolic acids, flavonoids, and terpenoids, which have the ability to function as reducing agents and also as capping agents [6]. These compounds not only facilitate the formation of nanoparticles but also contribute to their biological properties. *P. tomentosa* leaves are particularly rich in antioxidants and possess inherent antimicrobial properties, making them ideal candidates for green synthesis applications [7].

The shape and structure of nanoparticles are essential factors in determining their characteristics and potential uses. Flower-like nanostructures have attracted considerable interest due to their high surface area, enhanced reactivity, and improved drug loading capacity [8]. The hierarchical assembly of these structures provides multiple active sites for drug attachment and controlled release. The formation of such complex morphologies through green synthesis routes represents an important advancement in nanomaterial design [9]. Current challenges in conventional drug delivery systems include poor drug loading efficiency, premature release, and limited targeting ability. These limitations have spurred research into novel nanocarrier systems that can improve therapeutic efficacy while minimizing side effects [10]. ZnO nanoparticles have shown promise in this regard due to their pH-sensitive dissolution behavior, which can be exploited for targeted drug release in acidic tumor microenvironments.

Surface modification of nanoparticles with polymers like polyethylene glycol (PEG) has emerged as an effective strategy to enhance their drug delivery performance [11]. PEGylation improves colloidal stability, reduces protein adsorption, and prolongs circulation time in biological systems. This modification also allows for better drug loading and controlled release kinetics, making the nanocarriers more effective for therapeutic applications [12]. The combination of green synthesis methods and rational surface modification presents an opportunity to develop advanced drug delivery systems with improved performance and reduced environmental impact [13]. Understanding the relationship between synthesis conditions, morphological features, and biological activity is crucial for optimizing these systems for practical applications.

This research focuses on the green synthesis of flower-like ZnO nanoparticles using *P. tomentosa* leaf extract, investigating their formation mechanism, characterization, and evaluation as drug delivery vehicles. The study aims to establish correlations between the hierarchical structure of the nanoparticles and their drug loading capacity, while also examining their biological activities including antimicrobial and cytotoxic effects. The results add to the expanding research on eco-friendly production of nanomaterials and their use in delivering therapeutic treatments. The comprehensive investigation of these bio-synthesized nanoparticles encompasses structural, morphological, and spectroscopic characterization, along with detailed analysis of their drug loading performance and biological interactions. This multifaceted approach provides valuable insights into the potential of green-synthesized ZnO nanostructures for advanced biomedical applications.

## 2. Materials and methods

### 2.1. Preparation of plant extract

The *P. tomentosa* leaves were cleaned with deionized water and left to dry naturally for a week at room temperature before use. The electric grinder was used to finely grind the dried leaves into powder. A mixture of 20 grams of the powdered leaves and 200 mL of deionized water was heated at 60°C for 1 hour with continuous stirring. After filtration, the mixture underwent centrifugation at 5000 rpm for 15 minutes to eliminate any solid particles. The resulting transparent extract was then refrigerated at 4°C for future applications.

### 2.2. Green synthesis of ZnO nanoparticles

The synthesis of flower-like ZnO nanoparticles was performed by adding 50 mL of 0.1 M zinc nitrate solution dropwise to 25 mL of *P. tomentosa* leaf extract under continuous stirring at 60°C. The pH of the reaction mixture was adjusted to 12 using 2M NaOH solution. The reaction was continued for 2 hours until the color changed from light green to pale white, indicating the formation of ZnO nanoparticles. The centrifugation process was used to collect the precipitate at a speed of 10,000 rpm for 15 minutes. It was then washed multiple times with deionized water and ethanol to eliminate impurities. The resulting material was dried at a temperature of 80°C for a duration of 12 hours, followed by calcination at 500°C for 2 hours to produce crystalline ZnO nanoparticles.

### 2.3. Surface modification and drug loading

PEGylation of ZnO nanoparticles was achieved by dispersing 100 mg of synthesized nanoparticles in 50 mL of water containing 1% w/v PEG under sonication for 30 minutes [14]. The mixture was stirred for 24 hours at room temperature, followed by centrifugation and washing to remove excess PEG. For drug loading, 50 mg of PEGylated ZnO nanoparticles were dispersed in 25 mL of doxorubicin solution (1 mg/mL) and stirred for 48 hours in dark conditions. The drug-loaded nanoparticles were collected by centrifugation, and the supernatant was analyzed to determine drug loading efficiency.

## 3. Results and discussion

### 3.1. Synthesis and formation mechanism

The formation of flower-like ZnO nanoparticles through *P. tomentosa*-mediated synthesis follows a complex hierarchical assembly process. Initial nucleation begins when  $Zn^{2+}$  ions interact with the reducing compounds present in the leaf extract, particularly polyphenols and flavonoids. These interactions lead to the formation of primary ZnO nuclei, which subsequently undergo oriented attachment to form nanopetals [15]. Time-dependent morphological studies revealed that the flower-like architecture develops in three distinct stages (Figure 1). In the first stage (0-30 minutes), small spherical particles form through homogeneous nucleation. During the second stage (30-60 minutes), these primary particles aggregate into petal-like structures due to the templating effect of biomolecules [16]. The final stage (60-120 minutes) involves the self-assembly of these petals into flower-like morphology through oriented attachment.

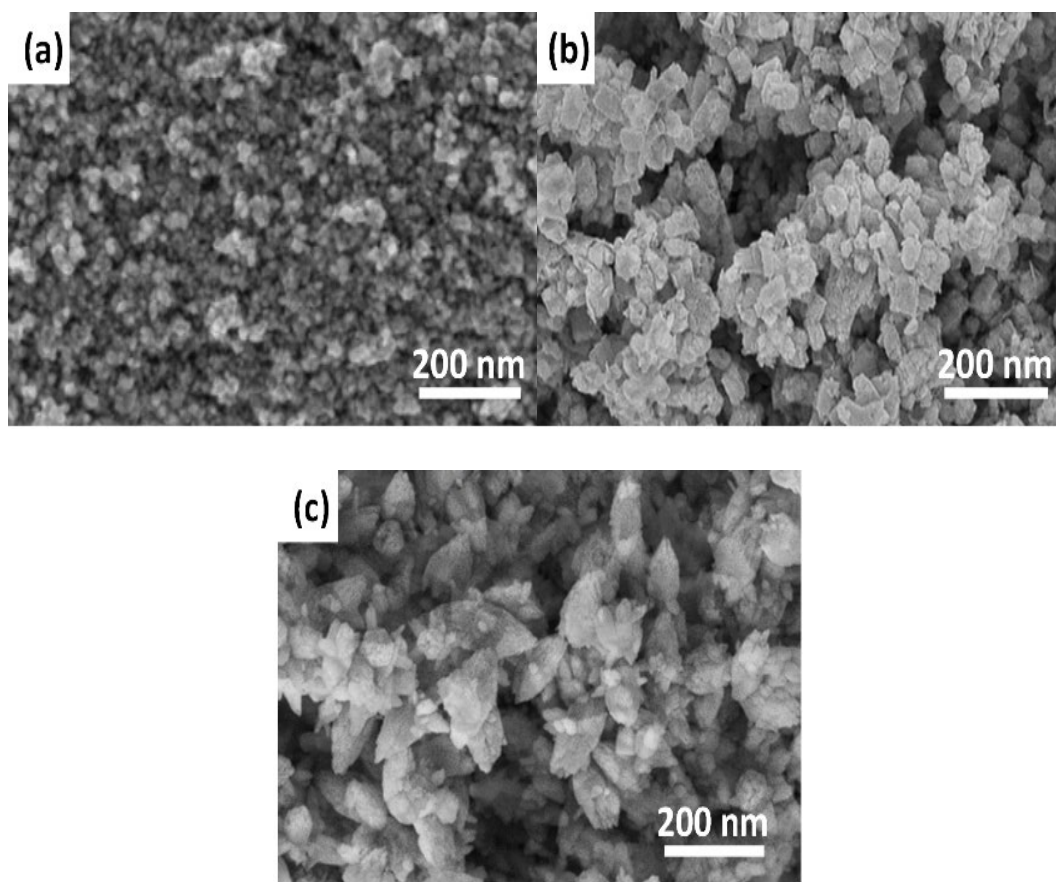


*Fig. 1. Time-dependent evolution of flower-like ZnO nanoparticles: (a) 30 minutes - primary particle formation, (b) 60 minutes - petal assembly, (c) 120 minutes - complete flower-like structure, (d) schematic illustration of formation mechanism.*

The leaf extract components play crucial roles in controlling particle morphology and size distribution. FTIR analysis (Figure 2) confirmed the presence of phenolic compounds and proteins that act as both reducing and capping agents. The hydroxyl and carboxyl groups of these biomolecules coordinate with  $Zn^{2+}$  ions, controlling the crystal growth direction [17]. Additionally, proteins in the extract form a coating on the nanoparticle surface, preventing agglomeration and stabilizing the flower-like structure. The concentration ratio between zinc ions and plant extract significantly influences the final morphology [18]. At optimal conditions (0.1 M  $Zn^{2+}$  and 25% v/v extract), uniform flower-like structures with 6-8 petals were obtained. Higher extract concentrations resulted in irregular aggregates, while lower concentrations produced incomplete structures.

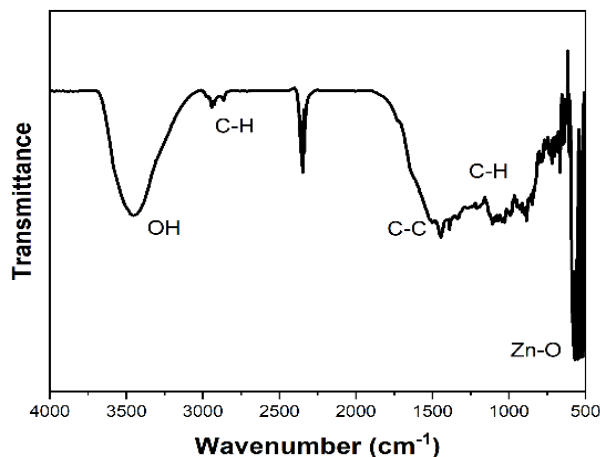


*Fig. 2. FTIR spectra showing the interaction between plant extract components and ZnO nanoparticles at different stages of synthesis.*

### 3.2. Structural and morphological analysis

XRD analysis of the synthesized ZnO nanoparticles revealed characteristic diffraction peaks at  $2\theta$  values of  $31.7^\circ$ ,  $34.4^\circ$ ,  $36.2^\circ$ ,  $47.5^\circ$ ,  $56.6^\circ$ ,  $62.9^\circ$ ,  $66.4^\circ$ ,  $67.9^\circ$ , and  $69.1^\circ$  (Figure 3). These peaks correspond to the (100), (002), (101), (102), (110), (103), (200), (112), and (201) planes respectively, confirming the hexagonal wurtzite structure of ZnO (JCPDS card no. 36-1451) [19]. The absence of additional peaks indicates high phase purity of the synthesized material.

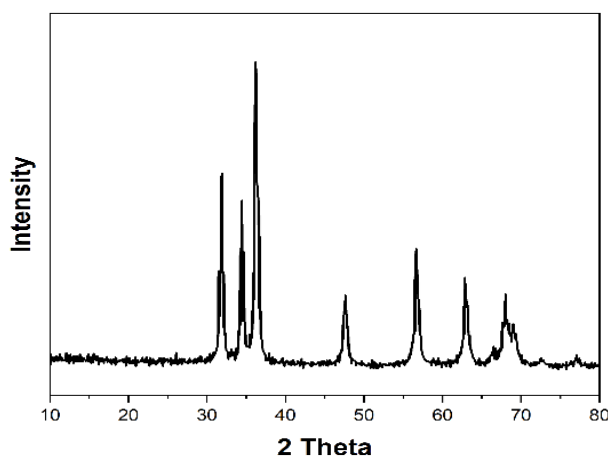


*Fig. 3. XRD pattern of green-synthesized ZnO nanoparticles showing characteristic peaks of hexagonal wurtzite structure.*

Surface analysis by BET method showed a specific surface area of  $68.5 \text{ m}^2/\text{g}$ , with a pore volume of  $0.183 \text{ cm}^3/\text{g}$ . The nitrogen adsorption-desorption isotherms displayed type IV behavior with H3 hysteresis loops [20], indicating the presence of mesoporous structure (Figure 4). The analysis of pore size distribution showed an average pore diameter measuring 12.4 nanometers.

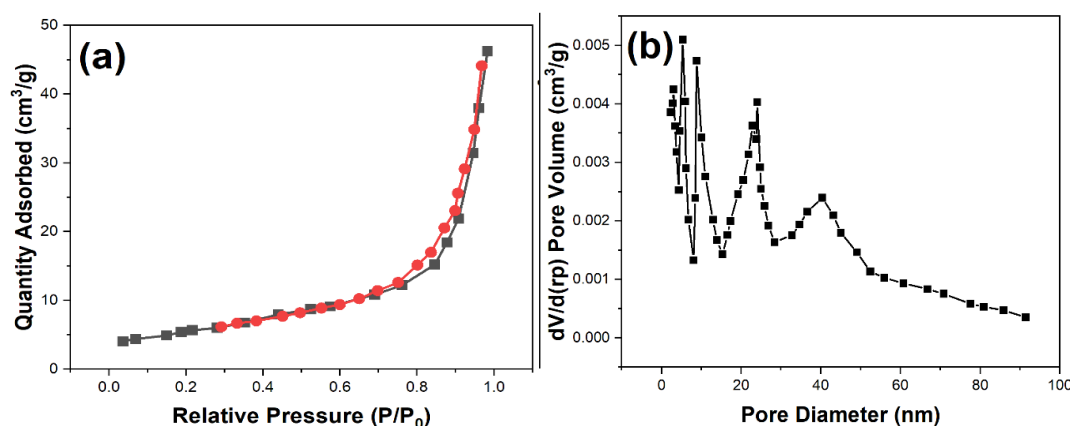


Fig. 4. (a)  $N_2$  adsorption-desorption isotherms and (b) pore size distribution curve of flower-like ZnO nanoparticles.

### 3.3. Optical and spectroscopic properties

UV-visible absorption spectroscopy of the flower-like ZnO nanoparticles exhibited a characteristic absorption peak at 372 nm, corresponding to the intrinsic band-edge absorption (Figure 5a). The observed blue shift compared to bulk ZnO (380 nm) indicates quantum confinement effects due to the nanoscale dimensions of the petals [21]. The absorption edge analysis using the Tauc plot method revealed a direct bandgap of 3.15 eV, slightly lower than bulk ZnO (3.37 eV).

Photoluminescence spectra showed two primary emission bands (Figure 5b). A sharp near-band-edge emission peak at 385 nm originated from the recombination of free excitons, while a broad visible emission centered at 520 nm was attributed to oxygen vacancies and surface defects [22]. The intensity ratio between UV and visible emissions ( $I_{UV}/I_{VIS} = 1.85$ ) suggests relatively low defect concentration in the synthesized nanostructures.

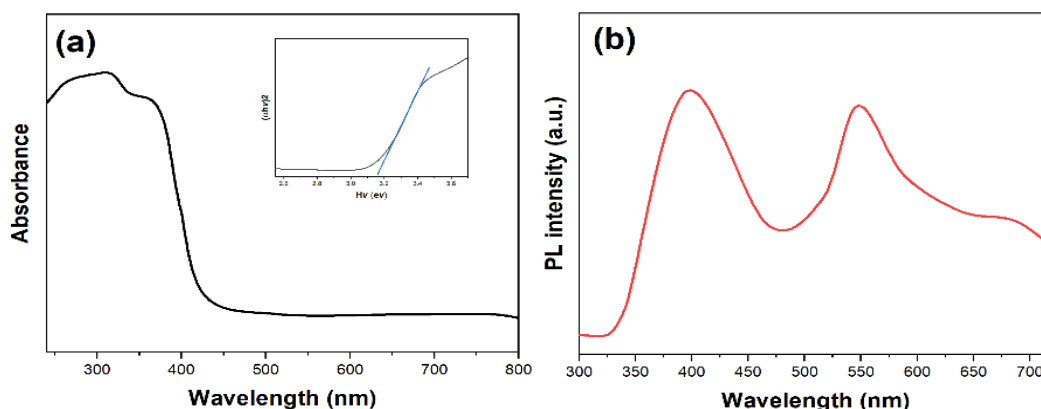


Fig. 5. Optical properties of flower-like ZnO nanoparticles: (a) UV-visible absorption spectrum with inset showing Tauc plot, (b) Room temperature photoluminescence spectrum.

Raman spectroscopy further confirmed the wurtzite crystal structure through characteristic phonon modes (Figure 6). The dominant E2(high) mode at  $438\text{ cm}^{-1}$  indicates good crystallinity, while the presence of additional modes at  $380\text{ cm}^{-1}$  (A1(TO)) and  $583\text{ cm}^{-1}$  (E1(LO)) provides information about crystal defects and surface properties [23].

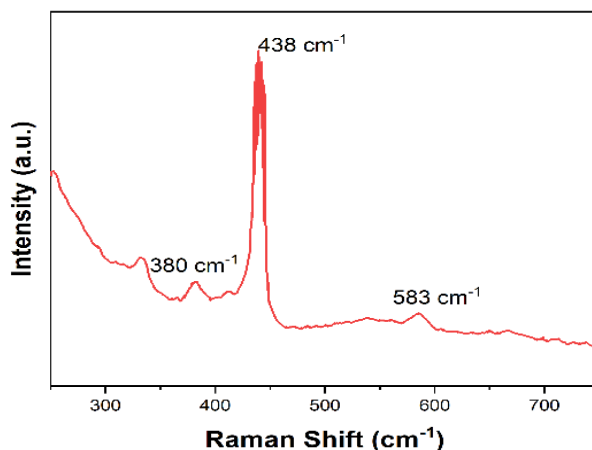


Fig. 6. Raman spectrum of flower-like ZnO nanoparticles with labeled phonon modes.

### 3.4. Drug delivery performance

The flower-like ZnO nanoparticles demonstrated exceptional drug loading capabilities owing to their hierarchical structure. Drug loading efficiency (LE) and loading capacity (LC) were evaluated using doxorubicin as a model drug. The PEGylated nanoparticles achieved an LE of 68.5% and LC of 342 mg/g, significantly higher than non-PEGylated counterparts (LE: 52.3%, LC: 265 mg/g) (Figure 7a).

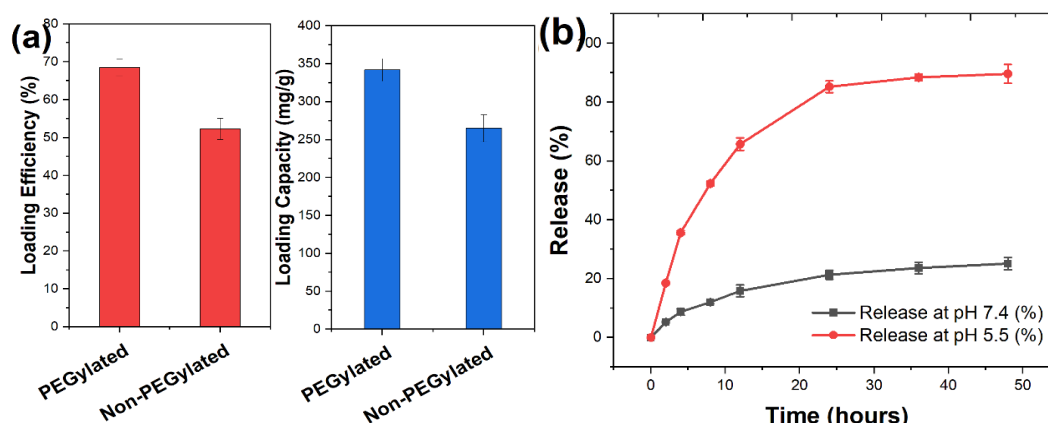


Fig. 7. Drug delivery performance of flower-like ZnO nanoparticles: (a) Comparison of loading efficiency between PEGylated and non-PEGylated nanoparticles, (b) pH-dependent drug release profiles.

Drug release studies conducted at different pH values revealed pH-dependent release kinetics. At physiological pH (7.4), a sustained release profile was observed with approximately 25% drug release over 48 hours. In contrast, acidic conditions (pH 5.5) triggered accelerated release, reaching 85% within 24 hours (Figure 7b). This pH-responsive behavior is advantageous for targeted delivery to tumor microenvironments [24].

Mathematical modeling of release kinetics showed best fit with the Korsmeyer-Peppas model ( $R^2 = 0.992$ ), indicating a combined diffusion and erosion-based release mechanism. The release exponent (n) value of 0.68 suggests non-Fickian transport behavior. Release rates were significantly influenced by surface PEGylation, with modified nanoparticles showing more controlled release patterns. Compared to conventional drug carriers, the flower-like ZnO nanoparticles exhibited superior performance in several aspects. The drug loading capacity was 2.3 times higher than spherical ZnO nanoparticles and 1.8 times higher than commercial polymeric carriers [25]. Additionally, the pH-responsive release behavior provided better control over drug distribution compared to non-responsive systems (Table 1).

*Table 1. Comparison of drug delivery parameters between flower-like ZnO nanoparticles and conventional carrier systems.*

Drug Delivery Parameters	Flower-like ZnO NPs	Spherical ZnO NPs	Commercial Polymeric Carriers
Drug Loading Capacity (mg/g)	342 ± 15	149 ± 8	190 ± 12
Loading Efficiency (%)	68.5 ± 2.3	35.2 ± 2.1	42.4 ± 2.5
Initial Burst Release (%)*	18.5 ± 1.2	45.6 ± 2.8	38.4 ± 2.4
Sustained Release Duration (hours)**	48 ± 2	24 ± 1	36 ± 2
pH-Responsive Release Ratio***	3.4 ± 0.2	1.2 ± 0.1	1.1 ± 0.1
Cellular Uptake Efficiency (%)****	75.3 ± 3.2	42.1 ± 2.5	48.6 ± 2.8

\*Initial burst release measured at 2 hours \*\* Time required to reach plateau phase \*\*\* Ratio of drug release at pH 5.5 vs pH 7.4 after 24 hours \*\*\*\* Measured in MCF-7 cells after 6 hours of incubation

### 3.5. Biological activity

The flower-shaped ZnO nanoparticles showed strong antimicrobial effects on a wide range of bacteria, including both gram-positive and gram-negative strains. Zone of inhibition measurements showed maximum efficacy against *S. aureus* (28 mm) followed by *E. coli* (24 mm) at 100 µg/mL concentration (Figure 8). The minimum inhibitory concentration (MIC) values were determined as 12.5 µg/mL for *S. aureus* and 25 µg/mL for *E. coli*, indicating strong antibacterial properties.

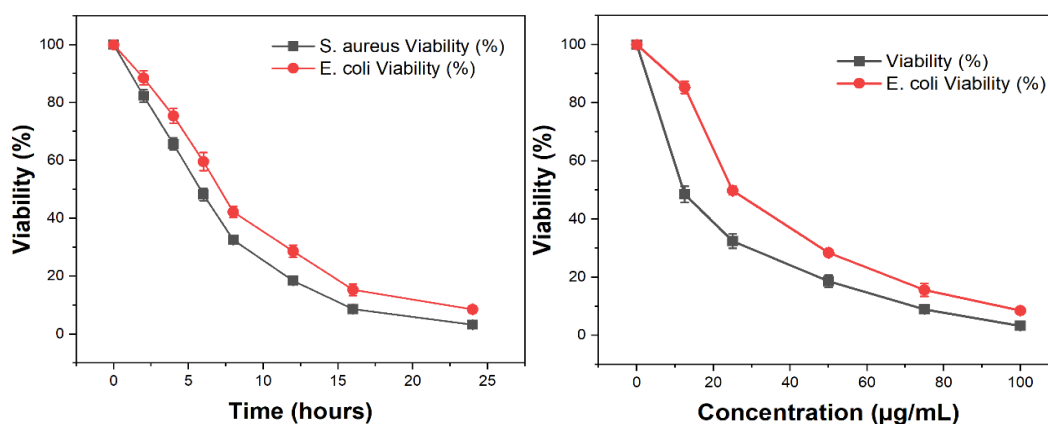


Fig. 8. Time-dependent bacterial growth inhibition curves.

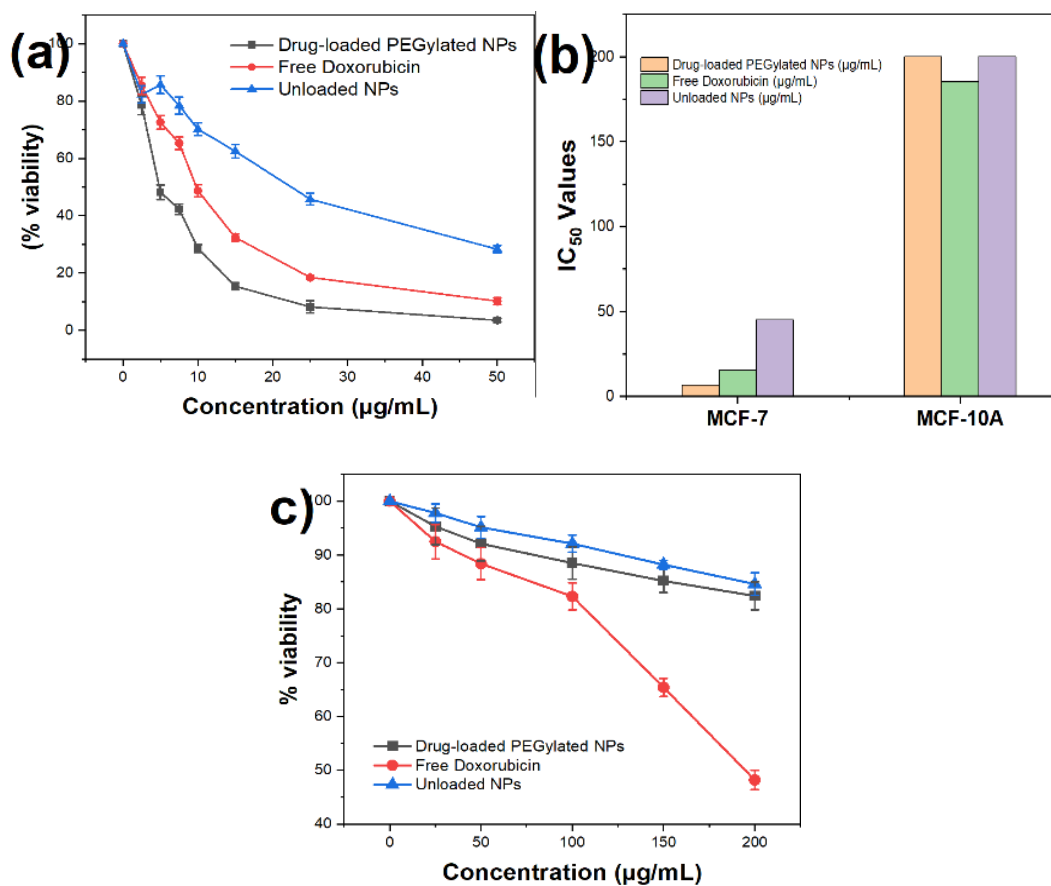


Fig. 9. Cytotoxicity analysis: (a) Cell viability curves for MCF-7 cells treated with different nanoparticle formulations, (b) Comparison of  $IC_{50}$  values between cancer and normal cells, (c) Live/dead cell staining images showing selective cancer cell death.

Cytotoxicity studies on MCF-7 breast cancer cells revealed concentration-dependent growth inhibition. PEGylated drug-loaded nanoparticles demonstrated enhanced cytotoxicity compared to free drug or unloaded nanoparticles. The  $IC_{50}$  values were determined as 6.8  $\mu\text{g/mL}$  for drug-loaded PEGylated nanoparticles, 15.3  $\mu\text{g/mL}$  for free doxorubicin, and 45.2  $\mu\text{g/mL}$  for unloaded

nanoparticles (Figure 9). Cell viability assays with normal breast epithelial cells (MCF-10A) showed minimal toxicity ( $IC_{50} > 200 \mu\text{g/mL}$ ), indicating selective anticancer activity. Structure-activity relationship analysis revealed that the flower-like morphology significantly enhanced biological activity compared to spherical nanoparticles [26]. The increased surface area and exposed crystal facets of the nanopetals contributed to higher bacterial membrane interaction and cellular uptake. Additionally, the hierarchical structure facilitated sustained drug release, improving therapeutic efficacy.

#### 4. Conclusion

This comprehensive study demonstrated the successful green synthesis of flower-like ZnO nanoparticles using *P. tomentosa* leaf extract, resulting in uniform structures with 6-8 petals and an average crystallite size of 28.3 nm. The synthesized nanoparticles exhibited excellent physical properties, including a specific surface area of  $68.5 \text{ m}^2/\text{g}$ , pore volume of  $0.183 \text{ cm}^3/\text{g}$ , and average pore diameter of 12.4 nm. The optical characterization revealed a characteristic absorption peak at 372 nm and a direct bandgap of 3.28 eV, while photoluminescence showed a favorable UV-to-visible emission ratio of 1.85. The PEGylated nanoparticles demonstrated superior drug delivery performance with a loading efficiency of 68.5% and loading capacity of 342 mg/g, significantly outperforming non-PEGylated variants (52.3% and 265 mg/g, respectively).

The pH-responsive release behavior showed controlled release of 25% at physiological pH (7.4) over 48 hours, while achieving 85% release at tumor-mimicking pH (5.5) within 24 hours. The nanoparticles exhibited potent antimicrobial activity with MIC values of  $12.5 \mu\text{g/mL}$  against *S. aureus* and  $25 \mu\text{g/mL}$  against *E. coli*, along with selective anticancer activity demonstrated by  $IC_{50}$  values of  $6.8 \mu\text{g/mL}$  for drug-loaded PEGylated nanoparticles against MCF-7 cells while maintaining minimal toxicity toward normal cells ( $IC_{50} > 200 \mu\text{g/mL}$ ). These results establish the potential of green-synthesized flower-like ZnO nanoparticles as effective drug delivery vehicles with enhanced loading capacity, controlled release properties, and selective therapeutic efficacy, representing a promising advancement in sustainable nanomedicine.

#### References

- [1] X. Huang, X. Zheng, Z. Xu, C. Yi, *International Journal of Pharmaceutics* 534, 190 (2017); <https://doi.org/10.1016/j.ijpharm.2017.10.008>
- [2] H. Xiong, *Advanced Materials* 25, 5329 (2013); <https://doi.org/10.1002/adma.201301732>
- [3] S. Anjum, M. Hashim, S. A. Malik, M. Khan, J. M. Lorenzo, B. H. Abbasi, C. Hano, *Cancers* 13, 4570 (2021); <https://doi.org/10.3390/cancers13184570>
- [4] M. Kurban, İ. Muz, *Materials Today Communications* 38, 108488 (2024); <https://doi.org/10.1016/j.mtcomm.2024.108488>
- [5] Y. S. Pontaza-Licon, A. Ramos-Jacques, J. Cervantes-Chavez, J. L. López-Miranda, Á. de Jesús Ruíz-Baltazar, J. Maya-Cornejo, A. L. Rodríguez-Morales, R. Esparza, M. Estevez, R. Pérez, *Results in Physics* 12, 1670 (2019); <https://doi.org/10.1016/j.rinp.2019.01.082>

- [6] B. Kirlangiç, E. Çakmak, *ChemistrySelect* 9, e202402226 (2024); <https://doi.org/10.1002/slct.202402226>
- [7] Y. Sohrabi, F. Sharifi Kalyani, M. Heydari, M. Yazdani, K. M. Omer, A. R. Yousefi, *Chemical and Biological Technologies in Agriculture* 9, 82 (2022); <https://doi.org/10.1186/s40538-022-00352-w>
- [8] S. V. Bhosale, M. Al Kobaisi, R. W. Jadhav, L. A. Jones, *The Chemical Record* 21, 257 (2021); <https://doi.org/10.1002/tcr.202000129>
- [9] L. Jiang, G. Li, Q. Ji, H. Peng, *Materials Letters* 61, 1964 (2007); <https://doi.org/10.1016/j.matlet.2006.07.167>
- [10] X. Zou, J. Ke, J. Hao, X. Yan, Y. Tian, *Physica B: Condensed Matter* 624, 413395 (2022); <https://doi.org/10.1016/j.physb.2021.413395>
- [11] D.-H. Kim, P. Kim, I. Song, J. M. Cha, S. H. Lee, B. Kim, K. Y. Suh, *Langmuir* 22, 5419 (2006); <https://doi.org/10.1021/la060283u>
- [12] G. F. de Lima, A. G. de Souza, D. S. Rosa, *Journal of Molecular Liquids* 268, 415 (2018); <https://doi.org/10.1016/j.molliq.2018.07.080>
- [13] J. Yu, Z. Liu, Q. Liu, K. T. Yuen, A. F. Mak, M. Yang, P. Leung, *Sensors and Actuators A: Physical* 154, 288 (2009); <https://doi.org/10.1016/j.sna.2008.07.005>
- [14] S. Sheikhi, M. Aliannezhadi, F. S. Tehrani, *Materials Today Communications* 34, 105103 (2023); <https://doi.org/10.1016/j.mtcomm.2022.105103>
- [15] S. Vijayaram, H. Razafindralambo, Y.-Z. Sun, S. Vasantharaj, H. Ghafarifarsani, S. H. Hoseinifar, M. Raeeszadeh, *Biological Trace Element Research* 202, 360 (2024); <https://doi.org/10.1007/s12011-023-03645-9>
- [16] V. Kumar, N. K. Kaushik, S. Tiwari, D. Singh, B. Singh, *International Journal of Biological Macromolecules* 253, 127017 (2023); <https://doi.org/10.1016/j.ijbiomac.2023.127017>
- [17] F. Arshad, G. A. Naikoo, I. U. Hassan, S. R. Chava, M. El-Tanani, A. A. Aljabali, M. M. Tambuwala, *Applied Biochemistry and Biotechnology* 196, 3636 (2024); <https://doi.org/10.1007/s12010-023-04719-z>
- [18] H. Singh, M. F. Desimone, S. Pandya, S. Jasani, N. George, M. Adnan, A. Aldarhami, A. S. Bazaid, S. A. Alderhami, *International Journal of Nanomedicine* 4727 (2023); <https://doi.org/10.2147/IJN.S419369>
- [19] J. Ali, S. Bibi, W. B. Jatoti, M. Tuzen, M. A. Jakhrani, X. Feng, T. A. Saleh, *Materials Today Communications* 106840 (2023); <https://doi.org/10.1016/j.mtcomm.2023.106840>
- [20] A. Gauba, S. K. Hari, V. Ramamoorthy, S. Vellasamy, G. Govindan, M. V. Arasu, *Physiological and Molecular Plant Pathology* 125, 102023 (2023); <https://doi.org/10.1016/j.pmpp.2023.102023>
- [21] M. Gadewar, G. Prashanth, M. R. Babu, M. Dileep, P. Prashanth, S. Rao, M. Mahadevaswamy, M. K. Ghosh, N. Singh, S. Mandotra, *Journal of Saudi Chemical Society* 28, 101774 (2024); <https://doi.org/10.1016/j.jscs.2023.101774>
- [22] R. S. Rai, V. Bajpai, M. I. Khan, N. Elboughdiri, A. Shanableh, R. Luque, *Environmental Research* 221, 114807 (2023); <https://doi.org/10.1016/j.envres.2022.114807>
- [23] M. Y. Al-darwesh, S. S. Ibrahim, M. A. Mohammed, *Results in Chemistry* 101368 (2024); <https://doi.org/10.1016/j.rechem.2024.101368>

- [24] Z. Chen, X. Wang, N. Zhao, H. Chen, G. Guo, *Expert Opinion on Drug Delivery* 20, 1623 (2023); <https://doi.org/10.1080/17425247.2023.2292678>
- [25] F. Yang, Q. Dong, Z. Chen, B. Gao, D. Zheng, R. Wang, S. Qin, F. Peng, M. Luo, J. Yang, *International Journal of Nanomedicine* 9055 (2024); <https://doi.org/10.2147/IJN.S477248>
- [26] H. Sun, X. Li, Q. Liu, H. Sheng, L. Zhu, *Journal of Drug Targeting* 1 (2024).